In-situ experiment on long-term behaviour of GFRP pipes under permanent bending

Cyril Douthe, Ioannis Stefanou

In-situ experiment on long-term behaviour of GFRP pipes under permanent bending

Cyril Douthe[a,*], Ioannis Stefanou[a]

[a] *Laboratoire Navier, École des Ponts ParisTech, Univ Gustave Eiffel, CNRS, France*

Abstract

The present study aims at studying the long-term behaviour of composites (GFRP) subjected to permanent bending. The specificity of this study largely rests on the original conditions of in-situ ageing of the specimens within an experimental structure of elastic gridshell, built in 2006 and disassembled in 2014. This prototype was made of rectilinear tubes which were elastically deformed into a 3D stable shape. The structural members constituted hence a unique set of relaxation tests in ambient conditions where a wide variety of curvatures were imposed by the 3D shape. After dismounting, the tubes were sorted according to their permanent curvature in the structure. They were then subjected to three kinds of tests: recovery, longitudinal bending and transverse bending tests. The results were then compared with those obtained during the construction of the prototype, before ageing, and with members aged under the same conditions but not mechanically loaded.

The experimental results confirm the usual recommendations for using composites in civil engineering, which suggest limiting the flexural stresses to 30% of the tensile strength to avoid damage or creep problems. At the same time, they confirm the safety and long-term robustness of the concept of double curvature structures obtained by elastic deformation of a composite plane grid.

Keywords: Glass Fibre Reingorced Polymers (GFRP), residual curvature, prestress, ageing, durability, relaxation

*Corresponding author

Email address: cyril.douthe@univ-eiffel.fr (Cyril Douthe)

1. Introduction

Key element in the use of Glass Fibre Reinforced Composites (GFRP) in Civil Engineering applications, such as buildings, bridges and facades, among others, is the long-term evolution of the mechanical properties of GFRP's. In this type of applications, GFRP's are inevitably subjected to permanent loads. As the applications of GFRP in construction is relatively limited up to date, the exact knowledge of the time-dependency of the fundamental mechanical parameters of GFRP is still not completely known. Laboratory experiments are frequently performed in order to improve the current state of knowledge. However, the duration of these experiments is usually limited, due to practical reasons. Moreover, theoretical analyses [such as 1, 2, 3, 4, among others, and references therein] provide useful insight and information, but still have to be validated using real, long-term experimental data.

The importance and novelty of this work relies on the use of experimental data from a real GFRP, elastic gridshell structure, which was built in 2006 and dismantled in 2014. Therefore, our experimental data involve time-dependent and ageing phenomena of 8 years under real environmental conditions. To our knowledge, these experimental data are unique and complete previous ones (see [5, 6]) in the sense that the structure is in a state of permanent bending under high stresses, which are characteristic in gridshell structures.

The gridshell structure was installed in Marne-la-Vallée in France (coordinates $48°50'31.6''$N, $2°35'19.1''$E), where detailed meteorological data exist and can be extracted from several databases. The overall dimensions of the gridshell were approximately 13m $\times$ 6m and it was made of long, rectilinear GFRP pultruded tubes of circular cross-section. The tubes were designed to deform elastically under large displacements and rotations [7]. Consequently, a wide variety of curvatures were developed due to the the three-dimensional (3D) shape of the gridshell and the imposed geometrical constraints (Figure 7). More details about the gridshell structure are given in Section 2.

Dismantling the gridshell structure after 8 years of service, gave us access to the time-dependent behaviour of its GFRP constituents and enabled us to study their strength reduction and stiffness change (creep/relaxation). It is worth noticing, that the available experimental data for the time-dependent behaviour of GFRP's is mainly based on accelerated creep tests of tubes of limited length. More specifically, starting from the 1950s a large amount of experimental data exists regarding the creep and fatigue response of GFRP [see 8, and references therein]. As the duration of most of the existing laboratory experiments are limited in time, accelerated characterisation techniques are frequently used in order to calibrate linear and non-linear viscoelastic theories and predict the long-term performance of composites under sustained loads. The majority of these experimental studies on creep have been performed in the aerospace and naval fields, and less in Civil Engineering, where the use of GFRP's seems to be a promising material [9, 10, 11].

1.1. Creep behaviour

Temperature and humidity are central factors for creep as they influence the viscosity of the GFRP matrix. Daniali [12] did an extensive parametric study of the short-term and long-term behaviour of GFRP T-shape beams varying the types of matrices (polyester/vinylester), the temperature (ambient temperature/$54°C$) and the geometry of beams (solid/cavity web). The author showed that the beams with vinylester matrix present less strength decrease at high temperature, longer creep life and smaller deflection compared with those of polyester matrix. However all specimens fully recovered after the removal of the applied load and no permanent deformation or damage was reported. An additional study was later conducted by Abdel-Magid et al. [13] on GFRP composites, with polyurethane matrix (PU) and epoxy matrix (EP). They observed that the shear properties of the matrix and the interfacial adhesive force between the matrix and the fibres is critical for the creep-failure strength. These works, among others, corroborate the importance of humidity and especially of temperature on the creep behaviour of GFRP.

In parallel, analytical models were proposed by Bank and Mosallam [14], based on experiments on plane portal frame structures made of FRP pultruded profiles. Following Findley's power [15] for the prediction of the viscoelastic behaviour, the time-dependent response of the FRP elements and the contribution of shear force were considered. They found a reduction of 35% for the long-term effective flexural modulus and a reduction of 46% for the long-term effective shear modulus. Regarding the short-term tests, the behaviour of the structure was linear-elastic under low load level, and the deflection was completely recoverable. However, when the load increased, the deformation was no longer recoverable, and non-linear effects were observed due to damage accumulation. These results were confirmed by Shao and Shanmugam [16], who also used the simplified Findley power law to estimate the tensile and shear modulus in a Timoshenko beam model. They found that the values of the time exponent in Findley's model for tensile creep, shear creep and creep deflection were almost equal and that the average could be used as a constant for the material studied.

More recently Sá et al. [17, 18] compared empiric and phenomenological formulations and found that Findley's power law, Bruger-Kelvin model and Prony-Dirichlet series presented good accordance between them. They have showed that the elastic strains increased by 30% after 50000 hours under a load level of 20% of the ultimate stress. They showed also that the power law, combined with the Euler–Bernoulli beam theory, gave a accurate prediction of deflections under bending loads up to 40% of the ultimate strength (slightly higher than the recommended normal service conditions where the load level is one third of the ultimate strength).

Similar approaches were then used for the investigation of pultruded GFRP on flexural creep by Yang et al [19], on creep buckling by Harries et al [20] and even on creep flexural-torsional buckling by Boscato et al [21]. In the three cases, Findley power law models were calibrated on experimental tests and showed good agreement with experimental results.

1.2. Relaxation and recovery

The effect of hybridisation on the creep and the relaxation of pultruded composites (glass fibre and carbon fibre with epoxy matrix) was evaluated by Barpanda and Raju [22]. The analysis of the data showed that the creep compliance and the relaxation modulus of flexure were independent of the type of fibres and the configuration of the composites. Zaoutsos et al. [23] and Guedes et al. [24] studied the modelling of the non-linear behaviour of composites, in tension and in bending, respectively. The formulation developed by Schapery was used in those researches and the established models were in good accordance with the test results. Then Al-Haik et al. [25] investigated the mechanical behaviour of carbon/epoxy composites. They set up a model with the parameters obtained from the relaxation tests and used them for the prediction of creep behaviour. The prediction was found consistent with the experimental data in short-term at low temperature.

More recently, advanced models tend to go beyond Findley power law and to differentiate the behaviour of the matrix and the fibres like in Cardoso and Harries [26], which captures well both phenomenon creep and relaxation and seems a very promising direction for numerical modelling. Nedjar *et al* [3] for example used a fibre breakage equivalent into a continuous damage model and observed that creep in fibre-reinforced composites is essentially due to the matrix constituent whose role is to deform and support stresses primarily in shear.

1.3. Environmental ageing

Nkurunziza et al. [27] studied the effects of sustained loads and environmental ageing on the tensile properties of GFRP reinforcement bars. The residual strength of the bars exposed to de-ionized water stayed almost the same. However, alkaline solution reduced the strength to 88% and 68% of the initial value under the stress level of 25% and 38% of the ultimate strength, respectively. On the contrary the modulus was not much influenced by the applied conditions.

Furthermore, an experimental study was realised by Sousa et al. [28] in order to identify the durability of GFRP pultruded profiles comparing accelerated

ageing and environmental ageing under Mediterranean climate. They observed that artificial ageing and environmental ageing could be correlated regarding their influence on aesthetic properties and also on mechanical properties, but in a less obvious manner. Carra and Carvelli [29] carried on the comparison of the different matrices: isophthalic polyester, orthophthalic polyester and vinylester. They confirmed that the effects of the artificial ageing are comparable with those of the environmental ageing but that it is hard to set up accurately a correlation between the two types of ageing.

1.4. Purpose and content of this work

According the previous literature review, there are few experiments combining creep or relaxation tests with environmental ageing and high bending stresses. From the separated effects, it seems that, if one follows the recommendations for civil engineering applications recommending stress levels below 30% of the limit strength, then long term deformation will stay recoverable and limited to approximately 40% of the instantaneous deformation. Moreover the effect of natural ageing will be limited. The purpose of the present study is thus to investigate the validity of these hypotheses and enable safe applications of GFRP composites in Civil Engineering.

The paper is structured as follows. Section 2 describes the original set up of the in-situ relaxation experiment. Three sets of tests are conducted. More specifically, recovery tests are presented in section 3, longitudinal bending tests in section 4 and transverse bending tests in section 5. A conclusion and a summary of the main results on the durability of structures made of pultruded tubes under pronounced bending closes the paper.

2. Methodology

2.1. Description of the prototype

The prototype of structure used in the present study builds on a structural concept of elastic gridshell magnified in 1975 by the work of Frei Otto *et al.*

for the Bundesgartenschau in Mannheim [30, 31]. This prototype is made of GFRP instead of wood and in that sense is the first GFRP elastic gridshell in the world. It had been presented in Douthe *et al* [7] (see Figure 1) where the advantages of GFRP compared to other Civil Engineering materials are detailed. It is made of a two way flat grid whose members are tubular pultruded profiles (with a 42mm outer diameter and a 35mm inner diameter) connected with swivel scaffolding elements that insures that the whole grid has no shear rigidity. Then as the tubes are very slender (the longest reach 13.2m), the grid can be deformed elastically by bending into a three dimensional shape (about 3.5m high for a 6.7m span). After deformation, this shape has been stabilised through the adding of a third direction of members that braces the grid and confers it its shell-like behaviour. The displacements occurring during the life time of the structure are thus approximately two orders of magnitude lower than those required for the forming of the grid. It can therefore be considered that this highly hyperstatic structure constitutes a unique but complex relaxation test on initially straight members that are forced to remain in given curved shapes. This assertion will be verified later in section 3.4 by simulating long term deformation of the shape according to the evaluated creep parameters.

Figure 1: View of the uncovered elastic gridshell.

2.2. Description of environmental conditions

The gridshell has been built in February 2006 and remained uncovered until March 2008 where a PVC textile cover was installed. The product used is a *Serge Ferrari Precontraint 502* which has a 10% solar transmission and filters 100% of UVB. The gridshell was dismounted in September 2009: the cover was removed, then the third direction of beams, the hinges at supports were unfasten, while the grid was sustained in the air with a crane, and finally flatten (see Figure 2). The grid was then stored flat outdoor for six months and exposed to UV and rain . The gridshell was then rebuilt in March 2010 and covered again. It was definitively dismounted following the former procedure in January 2014 at the beginning of the present experimental campaign.

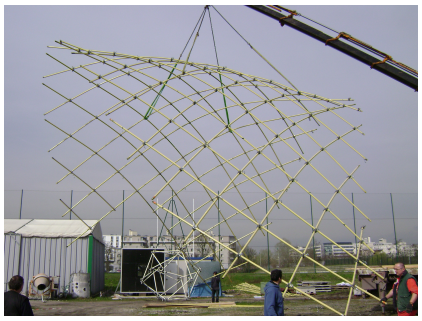

(a) Lifting of the grid

(b) Folded flat grid

Figure 2: Dismounting and unfolding of the structure.

In summary, during eight years, the gridshell members were subjected to:

- 24 months of permanent bending with UV and rain;
- 6 months of UV and rain without bending stresses;
- 64 months of permanent bending protected from UV and rain.

The gridshell shape was chosen, so that initial bending stresses are all below 35% of the limit strength of the members. Their evolution during time has not been monitored, but, from the visual aspect of the textile cover, where

no wrinkling was observed, it can be considered that the overall form did not change significantly during the life-time of the structure (again this is assessed a posteriori in section 3.4).

Outside temperature and air humidity were not registered but can be considered as very similar to that of Paris Montsoury meteorological station which is about 15km away from the campus and which has all data in open-access on *infoclimat.fr*.

2.3. Identification of members curvature

Considering the elastic gridshell prototype as a relaxation test, it is of first importance to have access to the actual curvatures of members in the structure. In [7], it had been shown that the numerical tool used for the simulation of the forming process was reliable. Reference values for "in-situ" curvature are thus taken from the numerical model of the structure. Figure 3 shows their distribution relatively to the maximum admissible curvature.

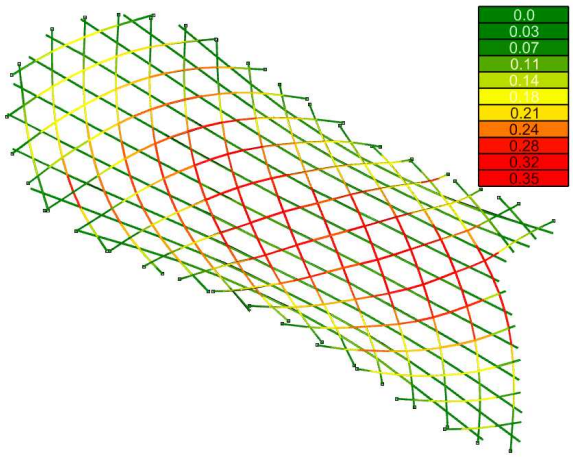

Figure 3: Initial ratio of curvatures in the prototype relatively to the maximum admissible curvature.

Immediately after dismounting of the structure, the beams were laid on the ground. They were in this state considered to be stress free, except the friction forces developed between the beams and the ground (concrete), which were

low. They were not straight anymore which evidenced stress relaxation in the structure during the life-time of the building. Their arched geometry was thus measured through a distance to the chord between the two ends. The precision of the measurement were about $\pm 2mm$ which is acceptable considering the fact that, for a $13m$ beam, the residual deflection was about $200mm$ at mid-span.

For estimating the residual curvature, this precision is however not sufficient. It was thus decided to extrapolate the measurements with a 6^{th} degree polynomial (with forced null values at the beams ends: $P(0) = P(L) = 0$). It can be seen on Figure 4 that the interpolation is very close from the measurements (the distance between the two curves is always below $1mm$). As a result, the residual curvature can be calculated at any point with a good reliability using the approximated polynomial of each deformed shape of beam.

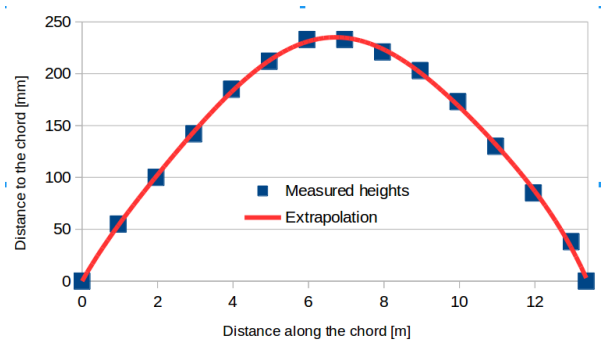

Figure 4: Measured residual heights and extrapolated model for beam n. 8.

Obviously the proposed method with the beams laying on the ground cannot capture any out-of-plane residual curvature. Yet the analysis of the 3D model of the gridshell structure reveals that the curves described by the beams centrelines are 3D-curves which are very close to planar curves. Indeed the curves are smooth, slowly varying and the maximum distance to the best fitting plane is generally below $10cm$ (for $13m$ beams with a height of around $3m$). The out-of-plane curvature is hence generally lower than 2% of the total curvature, especially in the areas where curvature is maximum (see Figure 5). Therefore, the reference "in-situ" curvatures of the beams will be those of the 3D curves.

Note that these curvatures are estimated from the numerical model and that their approximations are based on the inverse of the radius of the circumscribed circle of three successive nodes of the beam [32].

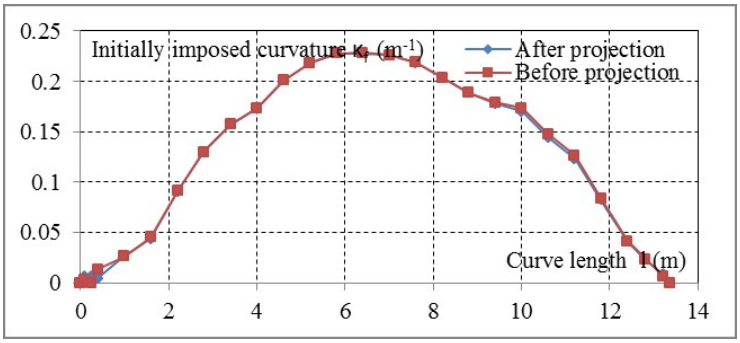

Figure 5: Comparison between 3D curvature and 2D curvature on the best fitting plane for beam n. 8.

2.4. Experimental campaign

Hence, for this in-situ experiment on long-term behaviour of GFRP pipes under permanent bending, the raw material is a set of tubes whose instantaneous characteristics had been characterised at time T_0 in [7] and which were subjected to a long term relaxation test. A wide variety of curvatures is explored thanks to the complexity of the shape of the elastic gridshell (see figure 3). The objectives of the following experimental campaign are:

- to determine the amplitude and nature (reversible or not) of the residual deformations of the members and to relate them with the "in-situ" curvatures;
- to determine whether mechanical properties (longitudinal and transverse) have been influenced by ageing and the level of "in-situ" curvature.

To this end, residual curvatures have been measured twice (first on the dismounting day and then five months later) following the procedure described in section 2.3. The evolution of these residual curvatures is compared to reference

creep tests in section 3. Afterwards, the members are sorted according to the level of curvature they were subjected to and submitted to bending tests in the longitudinal direction in section 4 and in the transverse direction in section 5. Both residual stiffness and strength are investigated and compared to the initial characteristics of the material.

3. Recovery tests

3.1. Reference test

In a creep/recovery or relaxation/recovery test, when the load is removed, there is an immediate recovery of elastic deformation, followed by some gradual recovery of creep deformation. Depending on the nature of creep (elastic or plastic), the long term recovery can be partial or total if the material was not damaged. In the present case, no continuous recording was available for the follow-up of residual deformation of the members and the determination of the nature of creep. It was thus decided to estimate the time-dependent recoverable deformation from a reference test made on the same material: same producer, same formulation with polyester resin and almost the same fibre content ($\approx 70\%$ of fibre) but different cross-section. The reference test is made on a pultruded rectangle 40x16mm while the members were made of circular hollow section. This reference creep test is actually a test conducted in the laboratory on a device dedicated to creep test under four points bending, the same as the one depicted in [7]. The $1m$ long specimen is loaded during a period of one month with a maximal moment equal to 30% of the specimen strength, which corresponds to a stress level similar to that of the gridshell members. Creep deformations are measured in the central part of the specimen which is under pure bending (the instantaneous elastic part is not shown.) The measured creep deflections are presented in Figure 6.

Findley's power law is then used to estimate the deformation after five years. The time dependant deformation are hence looked for in the following form: $m \cdot t^n$, where t stands for time in hour and where n and m are two material

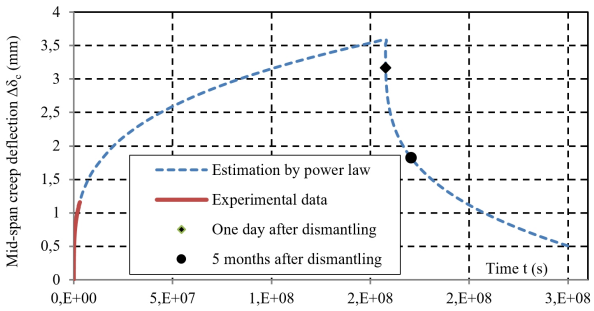

Figure 6: Reference creep test and extrapolation with Findley's power law supposing total recovery.

parameters to be identified. Here we found $m \approx 0,026$ and $n \approx 0,24$. Although different, these values are globally consistent with Sà *et al* [18] who give $m \approx 0,019$ and $n \approx 0,21$ at coupon scale and $m \approx 0,036$ and $n \approx 0,31$ at section scale.

Afterwards, the recovery is considered as the inverse process of creep. The curve of creep is thus reversed to figure the unloading period supposing a total recovery of creep deformation. The corresponding model is represented in Figure 6 by the dotted line. The residual mid-span deflection at one day and 5 months after unloading are then estimated with the model. So, in the case of total recovery of creep deformation, the residual deformation after five months should be approximately 42% lower than the residual deformation after one day. The comparison of the theoretical and experimental differences between the residual curvature of the gridshell members at day 1 and after five months should give us an indication on the nature of creep depending on the curvature level and "in-situ" ageing conditions.

3.2. Residual curvature at day 1

After the dismounting of the structure, the 34 members were measured one by one in at least ten points per length to estimate the residual curvature through a sixth order polynomial as explained in section 2.3. Then, the "in-situ" curvatures are calculated at characteristic points of the numerical model.

From the curvilinear abscissas of those points and the polynomial model, the residual curvature at corresponding points is then calculated. The scatter plot of residual curvature relatively to "in-situ" curvature is shown in Figure 7.

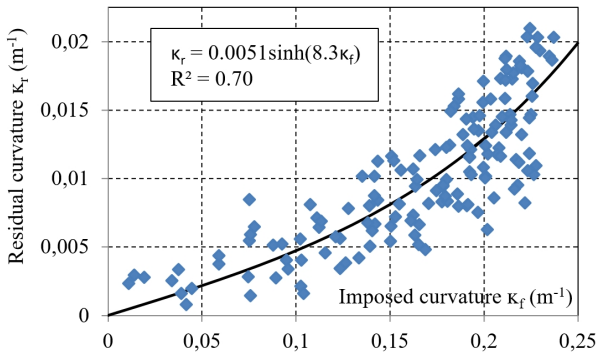

Figure 7: Residual curvature versus "in-situ" curvature at day 1.

In a first approximation, one could state that the residual curvature represents about 6.3% of the "in-situ" curvature. However, considering the fact that the relation between the two curvatures seems not strictly linear, one may try to find an empiric relation between them. To this end, Findley's power law is used here, as it is generally well adapted to predict the creep deformation of composites. For a given time, the deformation can be expressed in the form of a hyperbolic sine function of the imposed stress. Inspired by that, a hyperbolic sine model passing through the origin is fitted to the data of Figure 7 with a relatively satisfying coefficient of determination ($R^2 = 0.89$).

3.3. Estimation of recovery characteristics

On June 12th, 2014, 5 months after the dismantling of the structure, the pipes were thus measured again following the same method as at day 1. The results are shown in Figure 8, where obviously the scatter is higher than at day 1 because of the relative size of uncertainties. The residual curvature represents now about 4.0% of the "in-situ" curvature. Compared with the results at day 1, the relative decrease of residual curvature is equal to 37% of the curvature at day 1. Trying then to fit a hyperbolic sine function with the same argument

as the function at day 1 ($\kappa_{residual} = C_{5months} sinh(8.3\kappa_{in-situ})$), it can be seen that the amplitude of residual deformation passes from 0.0057 to 0.0032 which correspond to a reduction of 44%. Both estimations are close enough to the value obtained in the reference test (42%). It can thus be concluded that, probably, the creep deformations in the prototype will be totally recovered and that the permanent curvature and ageing have no major influence on the material behaviour, as will be confirmed in the following.

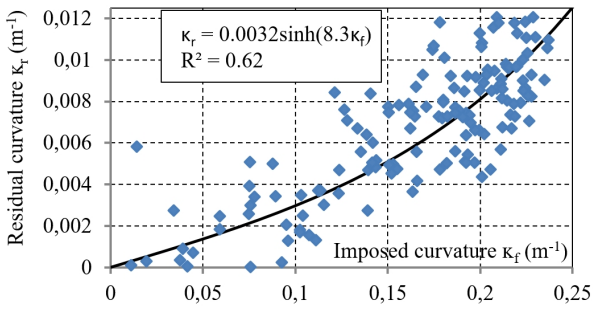

Figure 8: Residual curvature versus "in-situ" curvature after five months.

3.4. Discussion on the long term stability of the shape

The preceding measurements allow for the estimation of the long term behaviour of the members used in the prototype. Indeed, dependency in the curvature level was characterised in previous section 3.2 as a hyperbolic sine function of the curvature ($\sinh(8.3\kappa)$). Time dependency was also characterised in section 3.1 at 30% of the limit curvature as a Findley power law with characteristic values $m \approx 0,026$ and $n \approx 0,24$. Combining both and following the engineering approach of Sà *et al* [18], one can obtain an estimate of the variation of the longitudinal characteristics with time:

$$E(t) = E_0 \left(1 + 0.026 \frac{\sinh(8.3\kappa)}{\sinh\left(8.3\kappa_{30\%}\right)} \cdot t^{0.24}\right)^{-1} \quad (1)$$

Replacing the linear elastic material law by this roughly estimated material law in the software used for the simulation of the prototype, one is able to get the evolution of the shape and of the stresses through time. Figure 9 shows hence

the displacements induced by creep deformations after 10 years. Maximum displacements are located around the opening which is the known weakest point of the structure, they remain however very limited ($< 15mm$) and it can thus safely be concluded that the curvatures in the members did not change during the life time of the prototype.

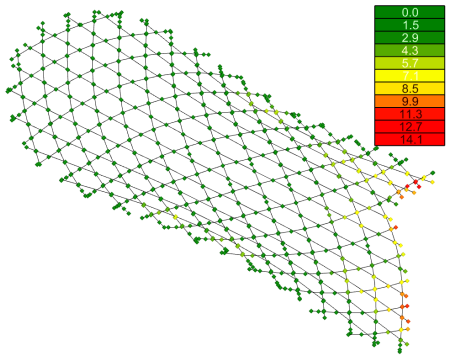

Figure 9: Displacement in mm induced by creep deformation under self stress after 10 years.

Interestingly, if one then compares the bending moments in the structure at the time of completion (see Figure 10a) and after 10 years (see Figure 10b), one notices that not only the maximum value drops of about 30% but also that, due to the stress dependency of the material law, the distribution of bending moments has become more uniform. From the structural designer point of view, the stress relaxation in the present case is hence in favour of safety, provided that it is not associated with a strength diminution, which is exactly investigated in the following.

4. Longitudinal characteristics

4.1. Experimental set-up

The tests on the long term longitudinal characteristics were realised in the laboratory facilities on an MTS testing machine with a capacity of 100 kN. They consist in four points bending tests in which a frame made of a double

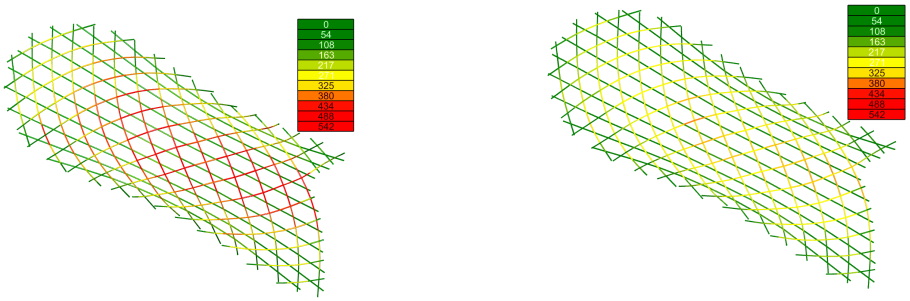

(a) Initial distribution

(b) After ten years

Figure 10: Evolution of the bending moments [Nm] in the prototype with time.

HEB140 steel profiles is fixed on the machine platform to adjust the span between the supports. Isostatic conditions are realised for the support and the loading element through steel cylinders with a diameter of 30 mm. The whole experimental set-up is illustrated in Figure 11. The length of the specimen is 1000 mm with an effective span of the specimens of 840 mm which corresponds to 20 times the diameter of the pipes. This ratio was considered sufficient for the contribution of shear stresses to the total deformation to be neglected (in the spirit of ISO standard for flexural properties of composites [33]).

Two series of tests are conducted: one for the identification of the elastic properties where the load is kept relatively low and one for the identification of the specimen ultimate strength. During the first series for the flexural modulus characterisation, the specimen is in direct contact with the supports and the loading elements, so that for the displacement measure no bias is introduced from the elasticity of the supports. The specimens are loaded up to 2 kN, which corresponds to approximately 20% of the estimated failure load and then unloaded. The load path was completely reversible.

On the contrary, during the tests for the ultimate strength characterisation, two layers of silicone were placed between the specimen and the supports as well as between the specimen and the loading elements to prevent local crushing (see Figure 12). In order to further prevent such failure, short steel pipes were also

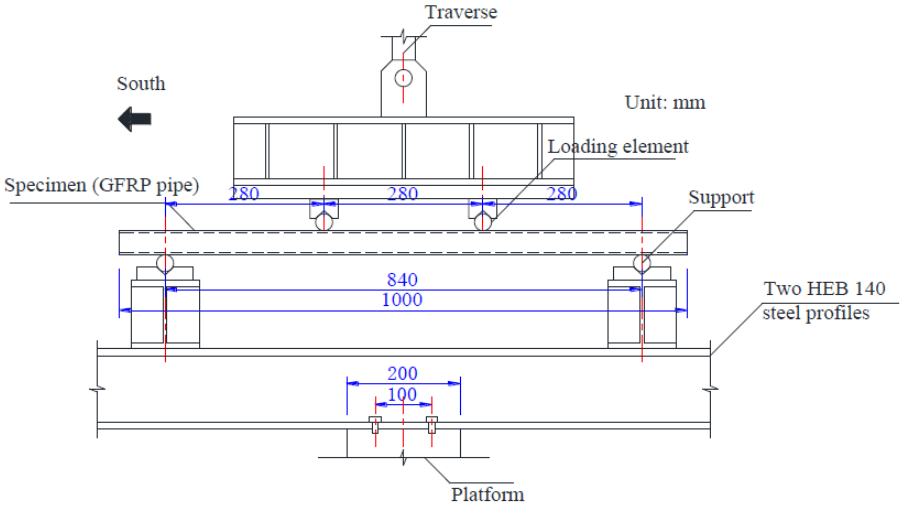

Figure 11: Four point bending test: scheme of experimental set-up.

put into the specimens at the positions correspondent to the loading's and the supports for reinforcement (Figure 12 right). These reinforcing disposals consist in steel pipes with a diameter of 32 mm (the diameter of the specimen is 35 mm) and a length of 40 mm. They are rounded and wrapped with tape in order to ensure their fitting with the specimen and to minimise stress concentrations. It was indeed observed during the adjustment of the ultimate strength tests, that, without the layers of silicone and the reinforcing disposals, the specimen broke at a load of 4.5 kN, and that, with the reinforcing disposals, the bearing capacity could reach 10 kN with failure modes similar to the initial one shown in [34].

Figure 12: Disposals to prevent local fracture: silicone layer and inner cylinder for supports.

4.2. Measuring devices

Before the tests, the dimensions (diameter and thickness) of every specimen were measured three times with the help of a vernier caliper. The averages of the three measurements were used as the final dimensions.

For the determination of the longitudinal bending modulus, displacement measurements are based on four linear variable differential transformers (LVDT), corresponding to the maximum number of channels available on the machine. For the ultimate strength, only the displacement of the machine is recorded. Two settings of LVDTs are used. In the first one, there is one LVDT below the specimen at mid-span, one below the loading frame in the South and two below the loading frame in the North in order to identify rigid body motion of the loading frame (see Figure 13).

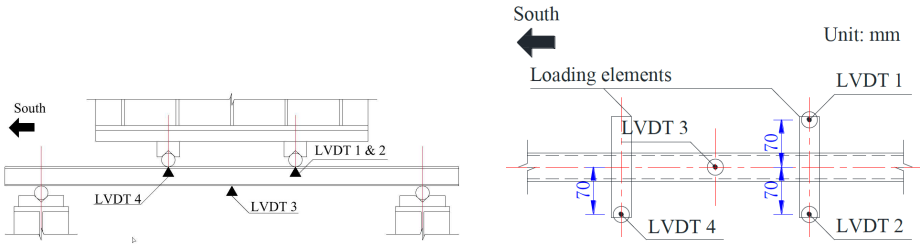

(a) Elevation (b) Plane view

Figure 13: First setting of LVDTs on the four points bending tests.

In the second setting, only 3 LVDTs are set, all below the specimen, one at mid-span and the other two at locations corresponding to the loading frame (see Figure 14). In this way, the displacements are measured on the lower fibre, the relative displacement between sides f_{load} and mid-span f_{max} is not biased by the ovalisation of the cross-section (contrary to the first setting). The longitudinal flexural modulus E_L is then easily calculated by standard Euler beam theory from the applied load P, the length l of the specimen and cross section inertia I:

$$E_L = \frac{3Pl^3}{648(f_{max} - f_{load})I} \tag{2}$$

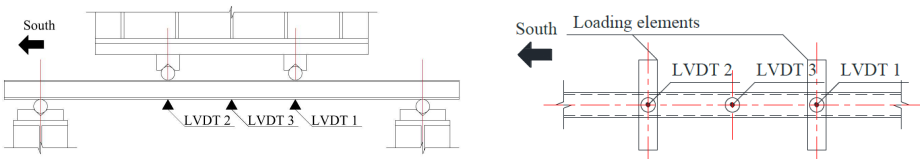

(a) Elevation (b) Plane view

Figure 14: Second setting of LVDTs on the four points bending tests.

4.3. Sorting of specimens

The proper identification of longitudinal bending properties required a specimen length of $1m$. Yet the lengths of the pipes in the gridshell range from $4m$ to $13m$. It is thus necessary to define a methodology to cut off the specimens from the whole members, so that the "in-situ" curvature of the specimen is as homogeneous as possible. We hence start identifying on the polynomial approximated model of the "in-situ" members where the point with the maximum curvature is located. The tubes are then cut symmetrically around that position into pieces of $1m$ with the help of a hacksaw.

Finally, for each resulting $1m$ specimen, the average curvature and the curvatures at both ends are evaluated. The comparison of this average value with the extreme values gives a measure of the curvature homogeneity along the in-situ specimens. It allows for a sorting of specimens into 4 classes according to the degree of variation of curvature:

1. The difference between the average curvature and the curvature at both ends does not exceed 10%.

2. The difference between the average curvature and the curvature at one end is comprised between 10% and 20%, while the difference between the average curvature and the curvature at the other end does not exceed 20%.

3. The difference between the average curvature and the curvature at one

end is comprised between 10% and 20%, while the difference between the average curvature and the curvature at the other end does not exceed 30%.

4. The difference between the average curvature and the curvature at one end exceed 30%.

The specimens are finally sorted in groups according to their average curvature or equivalently to their in-situ permanent stress relatively to the initial ultimate stress. The number of specimens of each class in each group is shown in Table 1. In each group, 8 specimens are selected in the highest possible class, 5 for the identification of the residual longitudinal flexural modulus, 3 for identification of the ultimate strength. These specimens are selected, so that their average curvature is as close as possible (less than 1% of the ultimate strength) from six target values: 0%, 15%, 20%, 25%, 30% and 35% of the ultimate strength.

Table 1: Inventory of specimens according to curvature level and homogeneity.

Class	$\leqslant 5\%$	5-10%	10-15%	15-20%	20-25%	25-30%	30-35%	$\geqslant 35\%$
1	0	0	0	2	15	61	56	3
2	0	1	3	25	20	14	2	0
3	0	2	13	18	5	0	0	0
4	25	34	17	4	1	0	0	0

4.4. Residual longitudinal bending stiffness

The complete campaign was conducted with the two LVDT settings which gave very similar results, with about 2% difference for each group which is about the uncertainty of the measure. Both settings can be considered to have the same accuracy, although the standard deviation of measurements with the second one is more homogeneous (close to 2%). The second setting avoids the bias of tube ovalisation, it is therefore chosen for the rest of the study. The average longitudinal flexural moduli calculated with the second setting (Figure 14) of each group of specimens is shown in Figure 15.

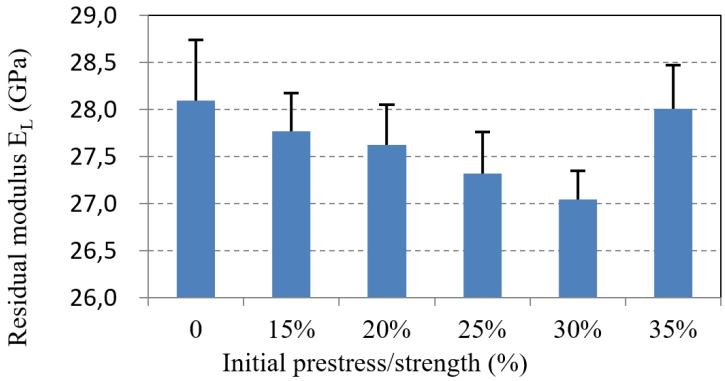

Figure 15: Residual longitudinal bending stiffness.

Looking into the results of Figure 15, it is observed that the residual longitudinal bending modulus decreases with the permanent stress level until 30% of the ultimate strength (about 4%). This conclusion is similar to that of Khan and Kim [35]. However, the average modulus of the last group, the one with a highest stress is almost equal to that of the reference specimen (the 0% group). A quick ANOVA on the whole set of data confirms that, from a statistical point of view, a few percent decrease is probable with the relative level of prestress defined by the ratio initial stress/strength.

The average modulus of each group is then compared with the initial value before ageing [34] (values presented here are slightly different from those of the initial publication as they have been corrected taken into account the actual characteristics of the cross sections and not those of the manufacturer). These values are summarised in Table 2. There is thus no effect of ageing (at that time scale and in those use conditions) and, statistically no significant effect of permanent stresses under those levels of bending stresses on the longitudinal stiffness.

4.5. Failure modes and the ultimate bending strength

During the ultimate strength tests, micro-cracking can be heard from a load of 2 kN (corresponding to about 20% of the limit strength), and the intensity

Table 2: Effect of ageing and permanent bending on the longitudinal bending stiffness.

Percentage of ult. strength (%)	0	15	20	25	30	35
Residual long. modulus (GPa)	28.09	27.77	27.63	27.32	27.04	28.01
Initial long. modulus (GPa)	28.11					
Difference (%)	0	-1.2	-1.7	-2.8	-3.8	-0.4

of the sound increases with the load level, similarly to the large scale bending test on the initial material [34]. Since two layers of silicone are placed between the specimen and the supports as well as between the specimen and the loading elements, it can reasonably be assumed that the cracks are due to the damage by bending of the material. As the failure load approached, the sound emissions become louder, which may be due to the local crushing or the generation and the propagation of the micro-cracks. A typical load-displacement curve is shown in Figure 16. As expected, the behaviour is linear elastic with a brittle fracture. The non-linear part at the beginning is due to the deformation of the silicone.

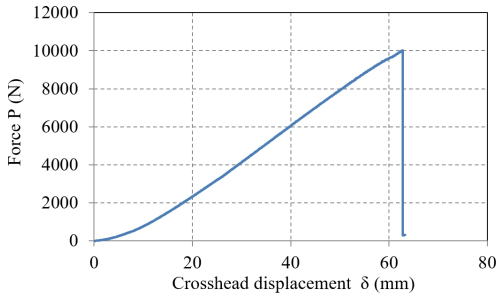

Figure 16: Typical brittle load-displacement curve of bending tests.

When the failure load is reached, the stress state in the specimen is very complex, especially due to its tubular nature: longitudinal stresses due to bending moments (Figure 17b), transverse compression at supports and loads due to shear forces (Figure 17a) and transverse stresses due to ovalisation (Figure 17c). Among the 18 specimens, three failure modes are observed: crushing at loading points (10 specimens), failure at mid-span (5 specimens) and longitudinal split-

ting (3 specimens). An illustration of each failure mode is shown in Figure 17.

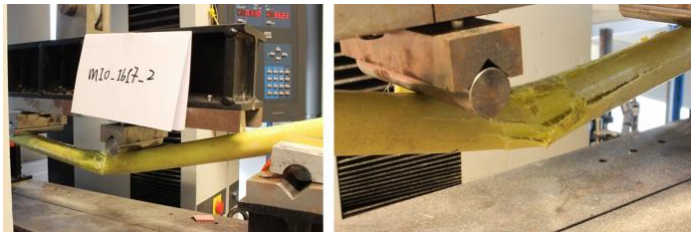

(a) Crushing at loading points

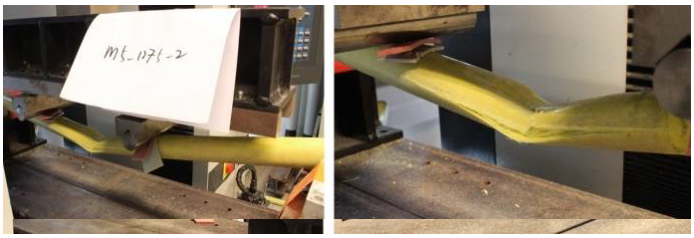

(b) Hinge at mid-span

(c) Longitudinal splitting

Figure 17: Three types of failure modes in bending.

The average failure loads of each group of specimens and of each failure mode are presented in Figures 18 and 19. Figure 18 shows that there is no obvious relation between the failure load and the "in-situ" stress level, especially because the scattering of values increases with the stress level. This scattering has also to be related to the importance of bifurcation phenomena in crack propagation and failure of structural systems where small different imperfections might lead to very different failure modes.

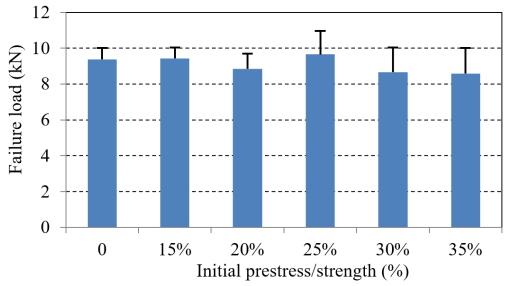

Figure 18: Failure load depending on the level of permanent stress.

In the same sense, Figure 19 shows very limited correlation between the ultimate load and the failure mode indicating that the ovalisation failure, transverse compression failure and longitudinal compression failure loads are very close to each other. Investigating then the correlation between the permanent stress level and the failure mode, it is found that all the specimens without permanent stresses fail due to crushing at loading points, while in the other groups, at least two other failure modes are observed. Since the last two failures modes are dominated by the transverse mechanical properties, it appears necessary to analyse more in depth the influence of permanent bending on transverse flexural properties, which is done in the next section.

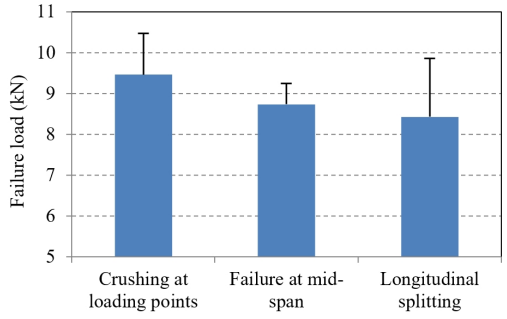

Figure 19: Failure load depending on the failure mode.

To complete the analysis of longitudinal properties, like for the stiffness, the ultimate longitudinal stresses of the aged specimens are compared to the initial ultimate stress [34]. Table 3 summarises the results of the comparison.

It can be seen that the ultimate strength of the unloaded members are similar: in average, ageing has no influence on the tube capacity. Some correlation is however observed between a loss of capacity and permanent bending stresses (at most 8.8%). This is in good agreement with previous observations and the fact that micro-cracking could be heard during the tests starting from 2 kN corresponding to 20% of the ultimate strength.

Table 3: Effect of ageing and permanent bending on the longitudinal ultimate stress.

Percentage of ult. strength (%)	0	0.15	0.2	0.25	0.3	0.35
Residual ultimate stress (MPa)	349	351	329	359	322	319
Initial ultimate stress (MPa)	350					
Difference (%)	-0.4	0.1	-6.0	2.6	-8.1	-8.8

5. Transverse characteristics

In order to understand the failure mechanism of the gridshell members, it is necessary to investigate their transverse characteristics. The stiffness and strength in the transverse direction are thus studied in the following.

5.1. Experimental set-up

Like longitudinal characteristics, transverse characteristics are investigated through bending tests at structure scale, through radial compression of cross sections of tubes as shown in Figure 20. This experimental setting is similar in proportion and procedure to the ones used by Gupta and Abbas [36] and Li *et al* [37], who have proved reliable in the identification of crushing properties of GFRP.

The same MTS testing machine as in section 4 is used, but this time with a load cell of 10 kN capacity. The alignment of the loading plates is guaranteed by the manufacturer with an unknown precision and there is no possibility for adjustment. The tests are displacement driven with a speed of 2 mm/min. All the specimens are loaded until rupture. All the tests are carried out at ambient

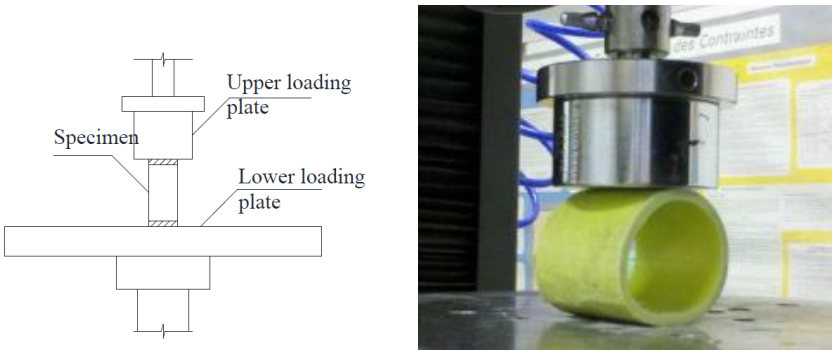

(a) Scheme of the transverse set-up

(b) Test under progress

Figure 20: Experimental set-up for transverse compression tests.

temperature ($26 \pm 1°$C). Notice that all the specimen are stored in the laboratory for more than 48 hours before the test. Notice also that the displacement measure is not "pure" and blends deformation of the experimental set up with deformation of the specimen (which are of a higher order of magnitude). It may however be supposed that the experimental set up displacements are independent of the specimen and time. Therefore, the results of the investigations on transverse characteristics presented here should be understood as relative rather than absolute.

5.2. Measurement devices

Before the tests, the dimensions (diameter and thickness) of every specimens are measured three times with the help of a vernier caliper. The averages of the three measurements are used as the final dimensions. During the tests, the total force P and the cross-head displacement δ are recorded (see Figure 21). Considering then the slenderness of the cylinder walls compared to the cylinder radius, the specimen can be considered as a circular beam in bending (stresses induced by normal and shear forces are negligible). Simple calculations of strength of materials allow for the evaluation of the transverse modulus E_T by [34]:

$$E_T = \frac{P}{\delta}\frac{3R^3}{t^3 L}\left(\pi - \frac{8}{\pi}\right) \tag{3}$$

where t is the thickness of the tube, L is its length and R the average radius. The maximum transverse bending stress σ_T^{rupt} is then obtained at the crown where the load is applied (point A in Figure 21) from the maximal load P^{rupt} by:

$$\sigma_T^{rupt} = \frac{6}{\pi}\frac{P^{rupt}R}{t^2 L} \tag{4}$$

The stress on the edge of the tube (point B in Figure 21) is significantly lower, about 43% and given by:

$$\sigma_T^{B} = \frac{6P^{rupt}R}{t^2 L}\left(\frac{1}{2} - \frac{1}{\pi}\right) \tag{5}$$

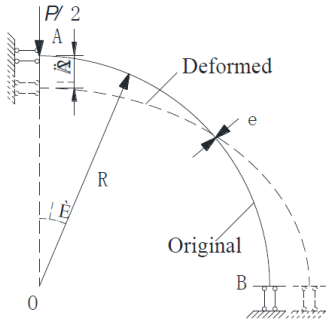

Figure 21: Scheme for the calculation of transverse characteristics.

5.3. Specimen

Following the sorting of the $1m$ specimens exposed in section 4.3, one specimen in each group is chosen with an in-situ curvature of 0%, 15%, 20%, 25%, 30% and 35% of the ultimate strength. These specimen are then cut into small cylinders with two lengths, 20 mm and 40 mm (3 specimens each), as in [34]. The idea is to find a compromise between the probability of damaging the specimen during cutting (which decreases with the length) and the influence of the non-parallelism of the loading plates (which increases with the length). From the campaign conducted here, it seems that the 40 mm specimens are more reliable as their average strength is 15% higher that that of 20 mm specimen. Both coefficients of variation are however equally high (about 30% of the average value).

5.4. *Residual transverse flexural modulus*

The average residual transverse flexural modulus of each group of specimens is shown in Figure 22, together with their standard deviation. No obvious relation can be found between the level of in-situ stress and the residual transverse modulus, and from a statistical point of view, considering standard deviation, one could conclude that there is no influence of permanent stresses.

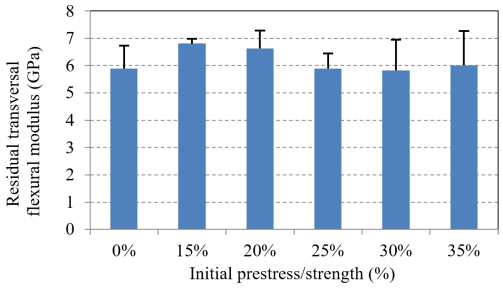

Figure 22: Residual Modulus in the transverse direction depending on the level of permanent stress.

Comparing then these values with the initial values [34] (see Table 4), one can see that in average, ageing has no influence on the transverse stiffness and that there is no coupling between ageing and permanent bending stress (at least for the considered level of stresses).

Table 4: Effect of ageing and permanent bending on the transverse modulus.

Group	0	0.15	0.2	0.25	0.3	0.35
Residual trans. modulus (GPa)	5.89	6.81	6.63	5.89	5.83	6.01
Initial value (GPa)	6.05					
Difference (%)	-3.4	11.6	8.8	-3.4	-4.5	-1.4

5.5. *Residual transverse flexural strength*

A typical force-cross-head displacement curve is shown in Figure 23. It can be seen from Equation (4) and (5) that the moment at the top/bottom of the specimen is superior to that at the two lateral points. Failure therefore starts

from the top/bottom of the specimen, but after the first hinge is formed, the section is still stable (with an hinge at point A, the structure in Figure 21 becomes isostatic) and it can resist additional load until new hinges form on the side. This residual capacity of the cross-section is clearly visible in Figure 23: the first drop of the curve corresponds to the rupture at the top/bottom of the specimen, it is accompanied by important sound, but the force can continue to increase until the failure of the lateral points. These results are in agreement with existing literature [36, 37].

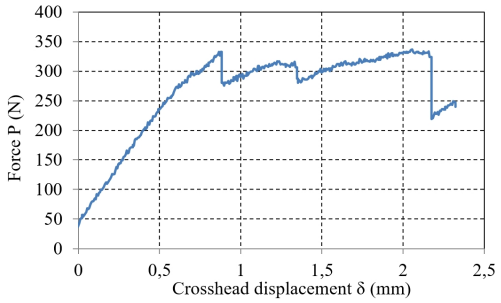

Figure 23: Load path of cross-section under transverse bending (Only the response of the sample for a force higher than 50N is reported, due to high tolerances of the apparatus and of the acquisition system in the beginning of the measurements.)

Table 5 presents detailed characteristics of the residual transverse strength: mean value σ_T^{mean}, minimum σ_T^{min} and maximum σ_T^{max} values as well as standard deviation σ_T^{stdv} for each group. The corresponding initial values [34] on the cross section before ageing have also been added for comparison. The spread of residual strength is much higher than that of residual stiffness, but so was also the spread of initial strength compared to initial stiffness. However for each criterion (mean, minimum and maximum, deviation), initial and residual values are comparable: there is thus no significant influence of ageing or permanent bending on the transverse bending strength.

Table 5: Effect of ageing and permanent bending on the transverse modulus.

Group	Init	0%	10%	15%	20%	25%	30%	35%
σ_T^{mean} [MPa]	16.1	15.3	22.2	26.6	18.4	17.9	16.9	18.2
σ_T^{min} [MPa]	8.8	9.5	15.9	25.2	9.8	8.4	6.5	8.2
σ_T^{max} [MPa]	28.7	18.5	26.6	30.2	31.8	24.1	25.4	29.4
σ_T^{stdv} [MPa]	6.9	5.1	3.9	1.9	8.1	5.9	6.7	10.5

6. Conclusions and perspectives

6.1. Summary of results

In this research, the long-term behaviour of GFRP pipes was studied based on an original in-situ experiment provided by the construction of the first GFRP elastic gridshell in the world. An empiric relation was established between the initially imposed curvature and the residual one. The specimens were then tested to obtain the residual mechanical properties of the material. By comparing the residual mechanical properties with the initial values, the effects of environmental ageing combined with permanent bending stress were evaluated. The main conclusions of this experimental campaign are given below.

- There has been a recovery of approximately 40% in the first 5 months, which indicates that, for the stress level tested in the prototype, deformations "remain" elastic and are fully recoverable.
- The residual modulus is always inferior to the initial value, with a difference ranging up to 4%. There is a little reduction of the longitudinal flexural modulus due to the environmental ageing combined with permanent bending stress, but it can be neglected considering the coefficient of safety during the design of the structure. It is however hard to establish a relation between the reduction of the longitudinal flexural modulus and the level of prestresss.
- No significant influence of ageing on the residual longitudinal strength was observed with a decrease of at most 8%.

- Similar observations were made for the transverse properties.

6.2. Perspectives for GFRP applications in Civil Engineering

This study confirms thus the feasibility and durability of GFRP structures for practical civil engineering applications, even when submitted to permanent bending stresses. Indeed, provided that the stress level remains below 30% of the ultimate strength, deformations remain recoverable and no significant damage occur. One may even say that in the specific case of elastic gridshells, relaxation is advantageous as part of the permanent stresses are released during the lifetime of the structure without stiffness or strength capacity loss.

Acknowledgement

The authors would like to thank the master student Mr Geng Shuai for performing most of the experiments and his work on this topic.

References

[1] H. L. Cox, The elasticity and strength of paper and other fibrous materials, British Journal of Applied Physics 3 (3) (1952) 72–79. doi:10.1088/0508-3443/3/3/302.

[2] I. Beyerlein, C. Zhou, L. Schadler, A time dependent micro-mechanical fiber composite model for inelastic zone growth in viscoelastic matrices, International Journal of Solids and Structures 40 (9) (2003) 2171–2194. doi:10.1016/S0020-7683(03)00021-0.

[3] B. Nedjar, N. Kotelnikova-Weiler, I. Stefanou, Modeling of unidirectional fibre-reinforced composites under fibre damage, Mechanics Research Communications 56 (2014) 115–122. doi:10.1016/j.mechrescom.2013.12.006.

[4] E. Dib, J. F. Caron, W. Raphael, I. Stefanou, F. Kaddah, Numerical analysis and investigation of short- and long-term behavior of unidirectional

composites, Journal of Composite Materials (2017) 002199831771335doi:10.1177/0021998317713355.

[5] T. Keller, Y. Bai, T. Vallée, Long-term performance of a glass fiber-reinforced polymer truss bridge, Journal of Composites for Construction 11 (1) (2007) 99–108. doi:10.1061/(ASCE)1090-0268(2007)11:1(99).

[6] T. Keller, N. A. Theodorou, A. P. Vassilopoulos, J. de Castro, Effect of natural weathering on durability of pultruded glass fiber–reinforced bridge and building structures, Journal of Composites for Construction 20 (1) (2016) 04015025. doi:10.1061/(ASCE)CC.1943-5614.0000589.

[7] C. Douthe, O. Baverel, J.-F. Caron, Gridshell structures with glass fibre reinforced polymer, Construction and Building materials 14 (9) (2010) 1580–89.

[8] D. W. Scott, J. Lai, A. H. Zureick, Creep behavior of fiber-reinforced polymeric composites: a review of the technical literature, Journal of Reinforced Plastics and Composites 14 (6) (1995) 588–617.

[9] J. Clarke, Structural Design of Polymer Composites: Eurocomp Design Code and Background Document, Taylor & Francis, 2003.

[10] F. Ascione, V. P. Berardi, L. Feo, A. Giordano, An experimental study on the long-term behavior of CFRP pultruded laminates suitable to concrete structures rehabilitation, Composites Part B: Engineering 39 (7-8) (2008) 1147–1150. doi:10.1016/j.compositesb.2008.03.008.

[11] L. Ascione, J.-F. Caron, P. Godonou, K. van IJselmuijden, J. Knippers, T. Mottram, M. Oppe, M. Gantriis Sorensen, J. Taby, L. Tromp, Prospect for New Guidance in the Design of FRP, 2016. doi:10.2788/851558.

[12] S. Daniali, Short-term and long-term behavior of two types of reinforced plastic beams, in: JNC 18, Ecole Centrale de Nantes, 2013.

[13] B. Abdel-Magid, R. Lopez-Anido, G. Smith, S. Trofka, Flexure creep properties of e-glass reinforced polymers, Composite Structures 62 (3-4) (2003) 247–253.

[14] L. C. Bank, A. S. Mosallam, Creep and failure of a full-size fiber-reinforced plastic pultruded frame., Composites Engineering 2 (3) (1992) 213–227.

[15] W. N. Findley, 26-year creep and recovery of poly(vinyl chloride) and polyethylene, Polymer Engineering & Science 27 (8) (1987) 582–585. doi:https://doi.org/10.1002/pen.760270809.

[16] Y. Shao, J. Shanmugam, Deflection creep of pultruded composite sheet piling, Journal of Composites for Construction 8 (5) (2004) 471–47.

[17] M. Sa, A. M. Gomes, J. R. Correia, N. Silvestre, Creep behavior of pultruded gfrp elements - part 1: Literature review and experimental study, Composite Structures 93 (10) (2011) 2450–2459.

[18] M. Sa, A. M. Gomes, J. R. Correia, N. Silvestre, Creep behavior of pultruded gfrp elements - part 2 analytical study, Composite Structures 93 (9) (2011) 2409–2418.

[19] Z. Yang, H. Wang, X. Ma, F. Shanga, Y. Ma, Z. Shao, D. Hou, Flexural creep tests and long-term mechanical behavior offiber-reinforcedpolymeric composite tubes, Composite Structures 193 (2018) 154–164.

[20] K. A. Harries, Q. Guoa, D. Cardoso, Creep and creep buckling of pultruded glass-reinforced polymermembers, Composite Structures 181 (2017) 315–324.

[21] G. Boscato, C. Casalegno, S. Russo, Creep effects in pultruded frp beams, Mechanics of Composite Materials 52 (1) (2016) 27–42.

[22] D. Barpanda, P. Mantena, Effect of hybridization on the creep and stress relaxation characteristics of pultruded composites, Journal of Reinforced Plastics and Composites 17 (3) (1998) 234–249.

[23] S. P. Zaoutsos, G. C. Papanicolaou, A. H. Cardon, On the non-linear viscoelastic behaviour of polymer-matrix composites, Composites Science and Technology 58 (6) (1998) 883–889.

[24] R. M. Guedes, A. T. Marques, A. Cardon, Analytical and experimental evaluation of nonlinear viscoelastic-viscoplastic composite laminates under creep, creep-recovery, relaxation and ramp loading, Mechanics of Time-Dependent Materials 2 (2) (1998) 113–128.

[25] M. Al-Haik, M. R. Vaghar, H. Garmestani, M. Shahawy, Viscoplastic analysis of structural polymer composites using stress relaxation and creep data, Composites Part B: Engineering 32 (2) (2001) 165–170.

[26] D. C. T. Cardoso, K. A. Harries, A viscoelastic model for time-dependent behavior of pultruded gfrp, Construction and Building Material 208 (2019) 63–74, special Issue 4th Brazilian Conference on Composite Materials (2018).

[27] G. Nkurunziza, B. Benmokrane, A. S. Debaiky, R. Masmoudi, Effect of sustained load and environment on long-term tensile properties of glass fiber-reinforced polymer reinforcing bars, ACI structural journal 102 (4) (2005).

[28] J. M. Sousa, J. R. Correia, S. Cabrial-Fonseca, Durability of glass fibre reinforced polymer pultruded profiles comparison between quv accelerated exposure and natural weathering in a mediterranean climate, Experimental Techniques (2013).

[29] G. Carra, V. Carvelli, Ageing of pultruded glass fibre reinforced polymer composites exposed to combined environmental agents, Composite Structures 108 (2014) 1019–1026.

[30] B. Burkhardt, M. Chaitos, J. Langner, W. Langne, G. Lubberger, IL13, Multihalle Mannheim, Erfahrung am Bauwerk, Institut für leichte Flächentragwerke (IL), 1978.

[31] E. Happold, W. Liddell, Timber lattice roof for the Mannheim Bundesgartenschau, The Structural Engineer 53 (3) (1975) 99–135.

[32] C. Douthe, O. Baverel, J.-F. Caron, Form-finding of a grid shell in composite materials, Journal of the I.A.S.S. 47 (150) (2006) 53–62.

[33] EN ISO 14125:1998 - Fiber-reinforced plastic composite - Determination of flexural properties.

[34] C. Douthe, Etude de structures élancées précontraintes en matériaux composites, application à la comception des gridshells, Ph.D. thesis, Ecole Nationale des Ponts et Chaussées (2007).

[35] F. Khan, Y. J. Kim, Time-dependent and residual behavior of pultruded gfrp beams subjected to sustained intensities and cold temperature, Cold Regions Science and Technology 74-75 (2012) 43 – 51. doi:10.1016/j.coldregions.2012.01.004.

[36] N. Gupta, H. Abbas, Lateral collapse of composite cylindrical tubes between flat platens, International Journal of Impact Engineering 24 (4) (2000) 329 – 346. doi:10.1016/S0734-743X(99)00173-6.

[37] S. Li, X. Guo, Q. Li, D. Ruan, G. Sun, On lateral compression of circular aluminum, cfrp and gfrp tubes, Composite Structures 232 (2020) 111534. doi:10.1016/j.compstruct.2019.111534.